Chemistry & Biology
Article

Probing the Selectivity and Protein·Protein Interactions of a Nonreducing Fungal Polyketide Synthase Using Mechanism-Based Crosslinkers

Joel Bruegger,[1,2,3] Bob Haushalter,[5] Anna Vagstad,[4] Gaurav Shakya,[1,2,3] Nathan Mih,[1,2,3] Craig A. Townsend,[4] Michael D. Burkart,[5,*] and Shiou-Chuan Tsai[1,2,3,*]
[1]Department of Molecular Biology and Biochemistry
[2]Department of Chemistry
[3]Department of Pharmaceutical Sciences
University of California, Irvine, Irvine, CA 92697, USA
[4]Department of Chemistry, Johns Hopkins University, Baltimore, MD 21218, USA
[5]Department of Chemistry and Biochemistry, University of California, San Diego, La Jolla, CA 92093, USA
*Correspondence: mburkart@ucsd.edu (M.D.B.), sctsai@uci.edu (S.-C.T.)
http://dx.doi.org/10.1016/j.chembiol.2013.07.012

SUMMARY

Protein·protein interactions, which often involve interactions among an acyl carrier protein (ACP) and ACP partner enzymes, are important for coordinating polyketide biosynthesis. However, the nature of such interactions is not well understood, especially in the fungal nonreducing polyketide synthases (NR-PKSs) that biosynthesize toxic and pharmaceutically important polyketides. Here, we employ mechanism-based crosslinkers to successfully probe ACP and ketosynthase (KS) domain interactions in NR-PKSs. We found that crosslinking efficiency is closely correlated with the strength of ACP·KS interactions and that KS demonstrates strong starter unit selectivity. We further identified positively charged surface residues by KS mutagenesis, which mediates key interactions with the negatively charged ACP surface. Such complementary/matching contact pairs can serve as "adapter surfaces" for future efforts to generate new polyketides using NR-PKSs.

INTRODUCTION

Polyketide natural products from filamentous fungi are highly diverse in both chemical structures and bioactivities, and they include current top-selling drugs, such as lovastatin (for lowering cholesterol), as well as potent toxins, such as aflatoxin and cercosporin (Crawford and Townsend, 2010; Hopwood, 1997). At the center of polyketide biosynthesis is the polyketide synthase (PKS), a multidomain enzyme complex. PKSs produce a huge variety of possible products via the controlled variation of building blocks, chain lengths, and modification reactions such as cyclizations. There are at least three types of PKSs in fungi (Shen, 2003). The nonreducing PKS (NR-PKS) subclass is an important, yet relatively less well-understood, family (Crawford and Townsend, 2010). NR-PKSs are involved in the synthesis of a wide spectrum of aromatic polyketides, including mycotoxins, such as aflatoxin (Figure 1D) (Watanabe et al., 1996) and zearalenone (Kim et al., 2005), that have a profound influence on agriculture (Huffman et al., 2010), current therapeutics, such as griseofulvin (Rhodes et al., 1961) (antifungal), and potential future therapeutics, such as bikaverin (anticancer) (Linnemannstöns et al., 2002; Ma et al., 2007) (Figure 1D). Similar to bacterial-derived tetracycline or daunorubicin metabolites (Otten et al., 1990; Perlman et al., 1960; Pickens and Tang, 2009), products from the fungal NR-PKSs have conjugated aromatic rings. These aromatic polyketides display an enormously rich spectrum of bioactivities (Hopwood, 1997); therefore, understanding how NR-PKSs generate polyketide diversity is significant with respect to (1) the identification and prediction of new polyketides based on the proteins responsible for their biosynthesis, which are encoded in the vast number of emerging sequenced microbial genomes, and (2) the generation of new bioactive polyketides by PKS engineering.

A typical NR-PKS contains a core set of six covalently linked catalytic domains (Crawford and Townsend, 2010) that execute the following generalized biosynthetic scheme (Figure 1B) (Cox, 2007; Crawford et al., 2008): the starter acyl carrier protein (ACP) transacylase (SAT) domain selects and loads the starter unit onto the acyl carrier protein. The chain is then transferred from ACP onto the ketosynthase (KS). Meanwhile, the malonyl-CoA:ACP transacylase (MAT) loads the extension unit building block from malonyl-CoA onto the ACP. Iterative rounds of decarboxylative Claisen condensations by KS domains synthesize a linear poly-β-keto intermediate, which is in turn cyclized and aromatized to form substituted aromatic rings by the product template (PT) domain (Figure 1C). The growing polyketide intermediate remains covalently attached to the ACP via the phosphopantetheine (PPT) prosthetic group during chain elongations and PT-catalyzed cyclizations. The final intermediate is transferred to the thioesterase (TE) domain, which catalyzes product release.

Over the past decade, many NR-PKSs have been cloned and heterologously expressed, and their products have been characterized (Crawford and Townsend, 2010; Huffman et al., 2010; Zhou et al., 2010). How one enzyme domain interacts with the

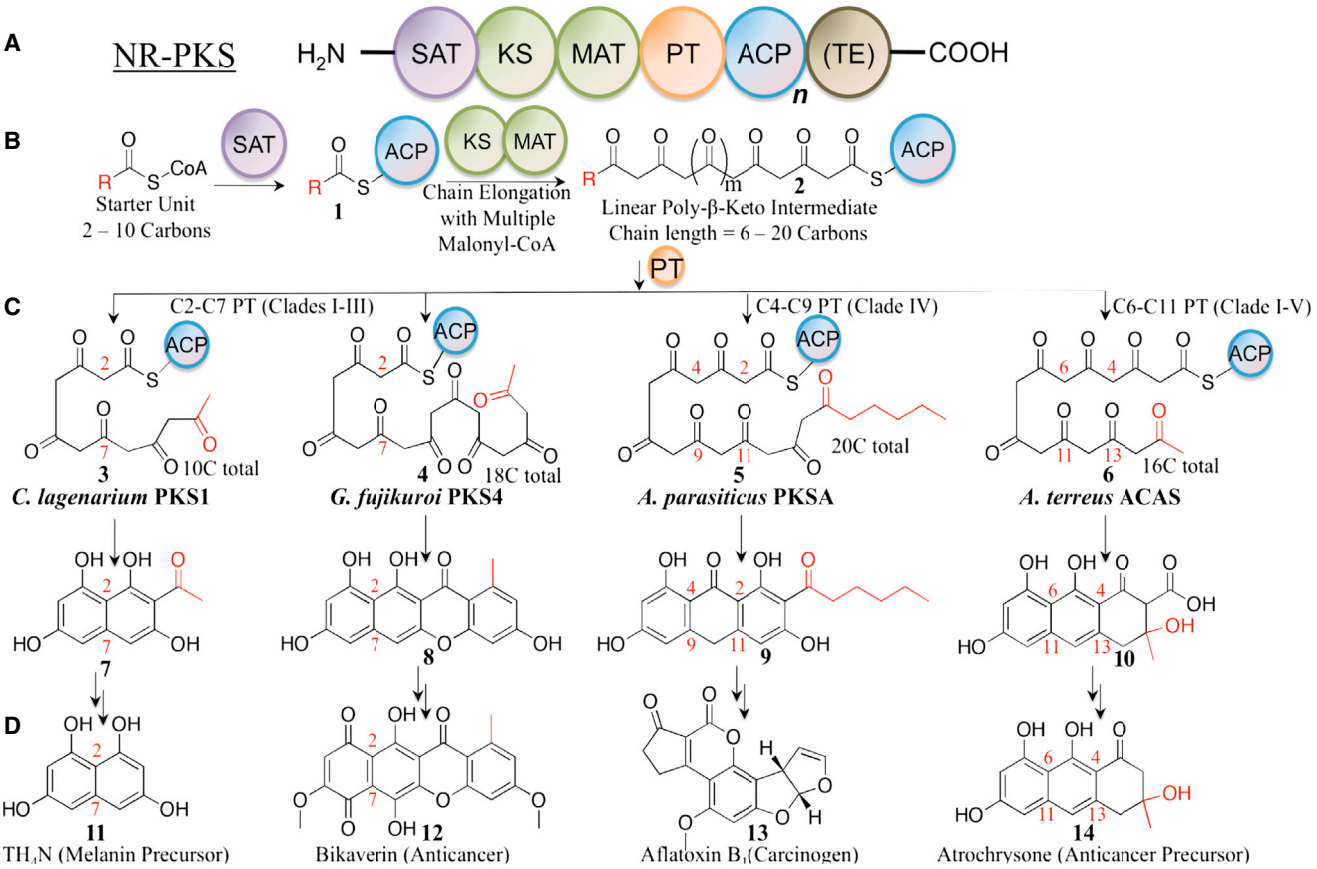

Figure 1. Polyketide Biosynthesis by Nonreducing Polyketide Synthases

(A) Domain architecture of a typical NR-PKS: there may be multiple ACPs (n = 1–3), and TE is optional (in brackets).

(B) NR-PKS enzymatic steps are initiated by the SAT domain with **1** (starter unit in red), followed by chain elongation by KS-AT (**2**).

(C) Cyclization is then promoted by PT in three patterns: C2-C7 (clades I–III, **3**-**4**), C4-C9 (clade IV, **5**), and C6-C11 (clade V, **6**).

(D) Additional enzymes modify the polyketide intermediates (**7**-**10**) and produce the final products (**11**-**14**).

other domains within the PKS megasynthase, however, remains largely unknown (Crawford et al., 2009; Korman et al., 2010). Prior engineering attempts indicate that protein•protein interactions are important in transporting the starter unit from SAT to KS, stabilizing the poly-β-keto intermediate, sequestering the linear chain in the KS and PT, and releasing the final cyclized product (Figure 1B) (Crawford and Townsend, 2010). The ACP mediates all enzymatic reactions that occur within the catalytic domains, and presumably, protein•protein interactions are essential for coordinating polyketide assembly. Specifically, docking interactions between KS and ACP domains should be important for starter unit selection, chain-length determination, and sequestration of the linear intermediate prior to cyclization. At this time, practically nothing is understood about ACP•KS interactions in NR-PKSs. Without such information, random domain shuffling has often resulted in abolished enzyme activity in microbial systems (Petkovic et al., 2002).

Although structures have been obtained for some individual NR-PKS domains (Crawford et al., 2009; Korman et al., 2010; Wattana-amorn et al., 2010), to date, the only related megasynthase structure reported is the 3.2 Å crystal structure of the porcine fatty acid synthase (FAS) (Maier et al., 2008), which bears little (<12%) sequence homology to NR-PKSs (Crawford et al., 2009). The mammalian FAS exists as a homodimer, both in the crystal structure (Maier et al., 2008) and in solution (Figure 2A) (Smith et al., 1985). The dimeric KS, dehydratase (DH), and enoyl reductase (ER) form the central "torso," and the MAT and ketoreductase (KR) monomers (the "legs" and "arms") are located on both sides of the torso. Our previous protein-sizing experiments showed that the SAT-KS-MAT tridomain of PksA exists as a dimer in solution (Crawford et al., 2009), which is architecturally similar to the KS-AT dimer found in porcine FAS (Figure 2B). As is the case for porcine FAS, the KS exists as a major part of the dimer interface in the overall PksA architecture, whereas the ACP of each monomer may interact alternately with each KS monomer during polyketide biosynthesis (Witkowski et al., 2004). Whereas in FAS, ACP presents the growing chain sequentially to the KR, DH, and ER domains following each extension to form a reduced methylene at the β-carbon position, in NR-PKSs the unaltered poly-β-ketide intermediate is fully extended in the KS before being transported to the PT domain for cyclization; the nature of ACP•KS interactions in NR-PKS remains a mystery.

In order to probe for protein•protein interactions between ACP and the catalytic domains within the PKS megasynthase, we

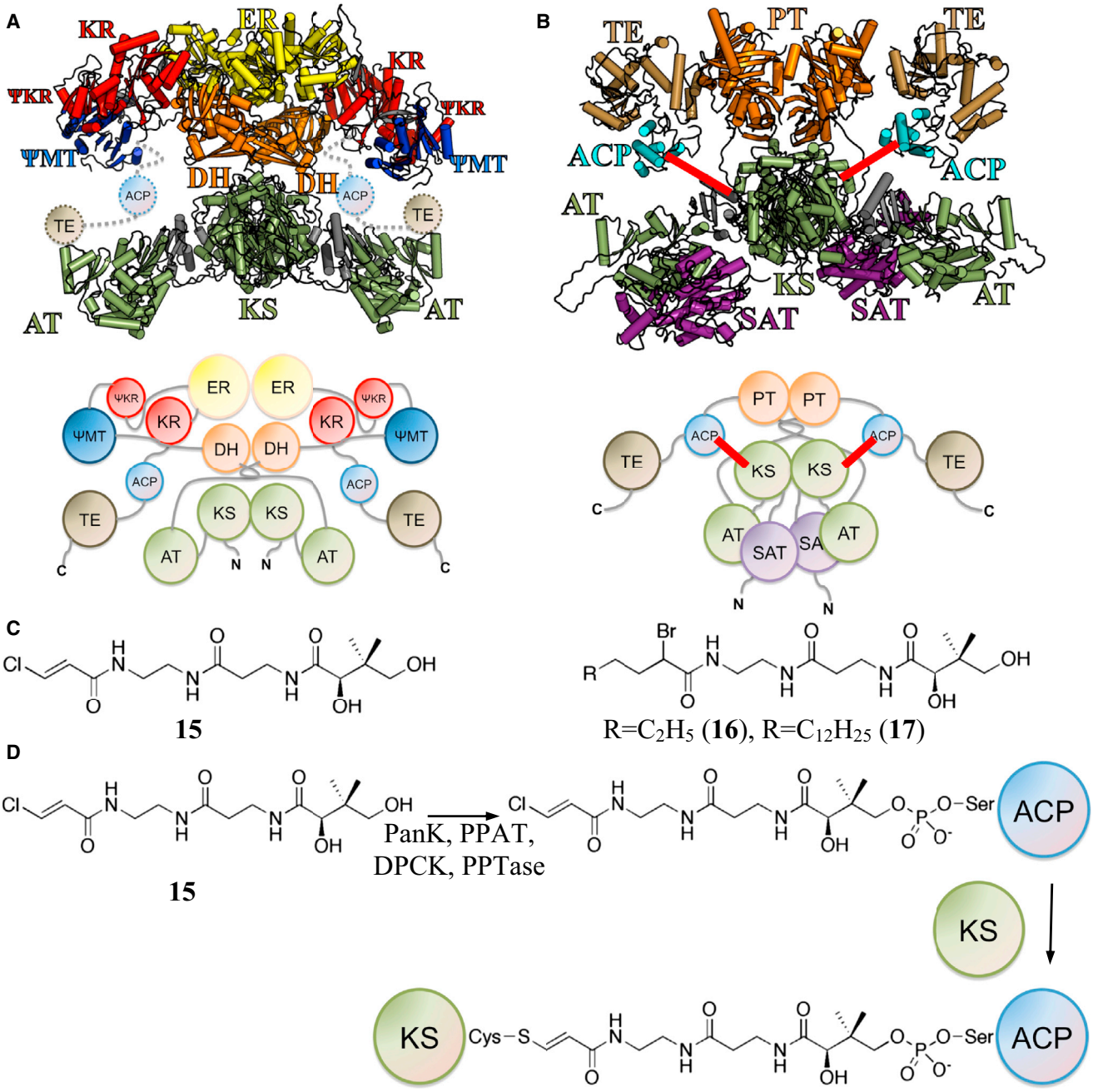

Figure 2. Potential Domain Architecture of NR-PKS Compared to mFAS and Crosslinking Reaction

(A) Crystal structure and cartoon of porcine FAS model as a homodimer, where KS is located at the center as a dimer.

(B) Protein sizing studies of PksA support an overall architecture similar to that of porcine FAS, where KS also exists as a dimer, and two ACPs on either side of the torso as shown in this homology model and cartoon. The crosslinking between KS and ACP is shown as red lines.

(C) Pantetheinylated probes with a chloroacryl **15,** 2-bromo hexyl **16**, or 2-bromo palmitoyl **17** chemical groups that target the nucleophilic cysteine of the KS domain.

(D) Chemoenzymatic attachment of **15**, **16**, or **17** to ACP is followed by KS crosslinking the nucleophilic cysteine of the KS domain.

have developed mechanism-based crosslinkers that can specifically bond the ACP to the KS (Figure 2C) (Haushalter et al., 2008; Kapur et al., 2008; Meier et al., 2006, 2010; Worthington and Burkart, 2006; Worthington et al., 2006, 2008, 2010). To attach the synthetic crosslinkers to ACP, a chemoenzymatic method using four enzymes—PanK, PPAT, DPCK, and a phosphopantetheinyl transferase (PPTase)—converts the pantetheine crosslinker analog to the coenzyme A-like species and appends it to the conserved serine residue of ACP (Figure 2D). When ACP forms a functional complex with the KS domain, the "warhead" group

is delivered to the KS active site and crosslinks to the Cys nucleophile (Haushalter et al., 2008; Kapur et al., 2008; Meier et al., 2006, 2010, Worthington and Burkart, 2006; Worthington et al., 2006, 2008, 2010). Our previous crosslinking studies showed that the degree of crosslinking is reliant on the strength of direct protein•protein interactions between ACP and the target partner of ACP (Meier et al., 2010; Worthington et al., 2010) and closely correlates to standard kinetic and thermodynamic techniques in revealing binding specificity (Worthington et al., 2006). Three crosslinkers (**15**, **16**, and **17**, Figure 2C) were developed that can be covalently attached to the ACP active-site Ser chemoenzymatically by the aforementioned four enzymes. They contain halide-leaving groups to enable nucleophilic attack by the KS active-site Cys, resulting in formation of a covalent link between ACP and KS (Figure 2D). The different chain lengths of the acyl moieties in **15**–**17** further enabled us to probe the substrate selectivity of KS.

In this work, ACP•KS interactions were probed by examining the crosslinking activity and compatibility between different domain combinations from PksA and Pks4, two 6-domain NR-PKSs (Figure 1A). The chemistries of PksA and Pks4 are shown in Figures 1B–1D; they are involved in the biosynthesis of aflatoxin and bikaverin, respectively. PksA extends and cyclizes a hexanoyl, a short fatty acid, starter unit to generate the 20-carbon product norsolorinic acid anthrone, whereas Pks4 uses the more common acetyl starter unit in the synthesis of the 18-carbon product prebikaverin/SMA76a (Figure 1). Two central hypotheses were tested for this study: (1) Cys-specific crosslinkers, such as **15**–**17**, will crosslink the ACP to the KS of an NR-PKS, and (2) crosslinking efficiency will correlate with the strength of domain•domain interactions. Here, we show that the first hypothesis is operable and that the starter unit specificity of KSs from different NR-PKSs is correlated with crosslinker specificity. We also demonstrate that only ACPs from NR-PKSs, but not from other PKS types tested, can be crosslinked effectively to the KSs. Furthermore, structure-based mutants of KS were prepared and studied to support the second hypothesis. The crosslinking studies between ACP and KS of PksA and Pks4 NR-PKSs elucidate the degree of protein•protein interactions between a matched or mixed pair of KS and ACP. The results identify structural features important for interdomain interactions that may be useful for future combinatorial biosynthesis efforts among mixed NR-PKS domain pairs.

RESULTS AND DISCUSSION

Chemoenzymatic Loading of 15–17 to NR-PKS ACPs

To ensure that the crosslinkers **15**–**17** (Figure 2C) can be functionally loaded onto the ACP domain of an NR-PKS, we cloned the stand-alone ACP domains from PksA and Pks4 as strep-tag fusions for affinity purification. The loading of pantetheine analogs **15**–**17** to ACP was monitored by MALDI, and the loading efficiency for 1 hr, 4 hr, or overnight incubations of the NR-PKS ACPs was compared to that of other ACPs, including the ACPs from modular type I PKS DEBS2, the type I FAS mycocerosic acid synthase, the type II *Escherichia coli* FAS, and the type II actinorhodin PKS (examples of loading as detected by MALDI are shown in Figures S2–S4 available online). The ACPs were selected to reflect the diversity of ACPs from both type I and II FASs and PKSs, with a sequence identity of 10%–24% to that of the PksA ACP. The loading efficiency of **15**–**17** was 100% for all apo ACPs tested within 1 hr, indicating that under these conditions, the loading of the crosslinker is independent of the affinity tag or the source of ACP (data not shown).

Crosslinking Is Probe Dependent Based on the Starter Unit Selectivity of KS

To ensure that the crosslinking between KS and ACP is specific, with no side reactions, we generated the N-terminal tridomain constructs, SAT(C117A)-KS-MAT (referred to as "S^0KM" throughout the text) of both PksA and Pks4, where the active-site Cys nucleophile of the SAT domain has been inactivated by mutation to Ala, ensuring that SAT would not compete with KS for crosslinking. We used the S^0KM tridomain construct because of insoluble expression of the KS monodomain. For the ease of downstream purification, we also cloned the S^0KM construct with an N-terminal 6-His tag cleavable by thrombin. Covalent crosslinking between the stand-alone ACP and the KS domain of S^0KM was monitored by an SDS-PAGE gel shift assay in which successful crosslinking results in an increase in the protein mass (Figure 3) (Haushalter et al., 2008; Kapur et al., 2008; Worthington et al., 2006, 2010). The 2-carbon substrate mimic, chloroacrylic pantetheine (**15**), crosslinks the ACP to Pks4 S^0KM, but not to PksA S^0KM (Figures 3A and 3B). In contrast, the 6-carbon mimic (**16**) and 16-carbon mimic (**17**) crosslink the ACP to both Pks4 and PksA S^0KM constructs (Figures 3A and 3B). Further, when **16** or **17** was used as the crosslinker, the ACP from Pks4 or PksA could be crosslinked to the S^0KM of either Pks4 or PksA, demonstrating that crosslinking between noncognate fungal NR-PKS domains occurred with nearly equal efficiency (Figures 3C and 3D) under the conditions tested. As a control experiment to confirm that the crosslinker is interacting exclusively with the KS, but not with SAT or MAT, the KS-specific inhibitor cerulenin was preincubated with S^0KM for 1 hr on ice before initiating the crosslinking reaction (Figure 3E). The addition of cerulenin resulted in the abolishment of crosslinking, confirming that the KS active-site Cys is essential for crosslinking. Additionally, when using an SKM construct in which the KS active-site Cys (C543 or C541 for PksA and Pks4, respectively) was mutated to Ala, no crosslinking occurred for either construct (Figure 3F). Therefore, for NR-PKSs, the crosslinking (and thereby protein•protein interactions between ACP and KS) is probe dependent, but not ACP dependent.

The above observation can be rationalized based on the starter unit selectivity of the KS domains. The PksA KS natively accepts a 6-carbon starter unit for chain elongation (Crawford et al., 2006), but not an acetyl unit, consistent with its specificity for **16** (the 6-carbon mimic), but not **15** (the 2-carbon mimic). In comparison, the Pks4 KS accepts a 2-carbon starter unit and subsequently conducts chain elongation until the intermediate reaches 18 carbons (Crawford et al., 2006; Ma et al., 2007). The 2-carbon mimic **15** is thus accepted by the Pks4 KS as the starter unit, whereas the 6-carbon mimic **16** is likely accepted by the Pks4 KS as a surrogate elongation intermediate. Similarly, the 16-carbon mimic **17** is likely accepted by both PksA and Pks4 KS domains as a pseudoelongation intermediate. The above result is significant, not only because it strongly supports that both SAT and KS domains (as opposed to only SAT) of PksA

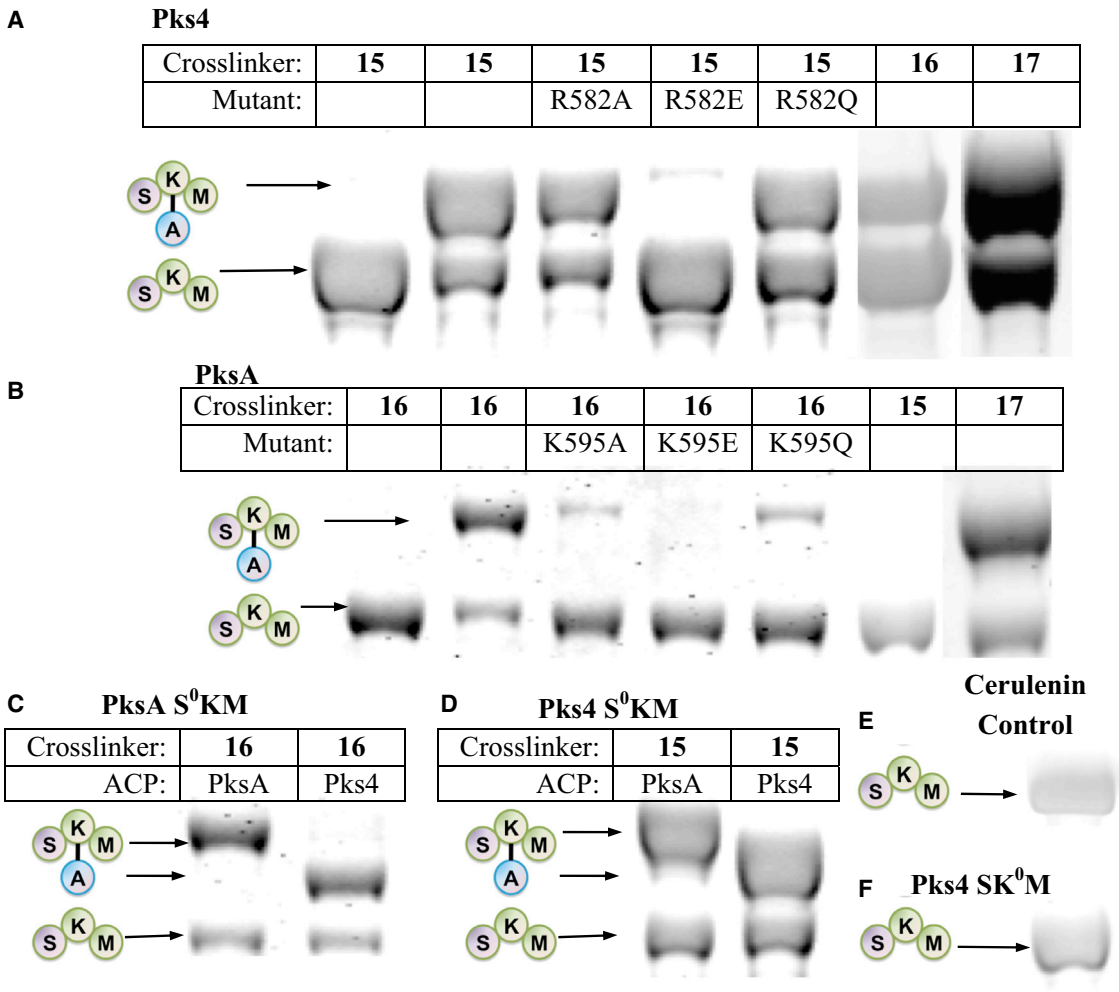

Figure 3. SKM Crosslinking Gels

(A) Pks4 ACP crosslinked to Pks4 S^0KM and KS surface mutants. Pks4 can crosslink by crosslinkers with acyl chains that range from 2–16 carbons (**15–17**). Surface mutations of Pks4 R582 (and K593 in Figure S1A) abolished crosslinking when the side-chain charge is reversed (R582E), a case that can be rescued by mutation to a polar amino acid (R582Q).

(B) PksA ACP crosslinked to PksA S^0KM and additional KS surface mutants. PksA requires a minimum of six carbons in the acyl chain of the crosslinkers (**16–17**). Reversing the charge of K595 (K595E) abolishes crosslinking, which can be rescued by mutation to a polar amino acid (K595Q). Similar results were found for K584 mutants (Figure S1C). When comparing (A) and (B) or PksA versus Pks4, the alanine mutation does not necessarily abolish protein-protein interactions. Rather, the reversal of charge (the mutation to glutamate) effectively abolishes the KS-ACP interactions. The difference is likely due to the distinct character at the protein interface of different PKSs.

(C) A comparison of PksA S^0KM crosslinked to PksA and Pks4 ACP, showing comparable crosslinking efficiency for the two ACPs from NR-PKSs.

(D) A comparison of Pks4 S^0KM crosslinked to PksA and Pks4 ACP, showing comparable crosslinking efficiency for the two ACPs from NR-PKSs.

(E) The negative control of cerulenin, which binds KS and prevents crosslinking. Our hypothesis that the KS active site must be accessible for crosslinking to occur is supported by the results. (F) As an additional control, the KS^0 mutant abolishes crosslinking, confirming that KS active site must be present for crosslinking to occur.

See also Figures S1–S6.

are selective for the hexanoyl starter unit but also because it demonstrates that probe specificity directly affects protein•protein interactions (as detected by crosslinking) between KS and ACP.

Crosslinking Ratio Is Correlated with Observed PKS Activity

The intact NR-PKS (six domains), as well as the tridomain S^0KM construct, exist as dimers in solution (Crawford et al., 2009). For either PksA or Pks4, the extent of crosslinking is dependent on the reaction conditions. Under our standard conditions (detailed in the Experimental Procedures) with a 1 hr incubation, only one subunit of the S^0KM dimer crosslinks to a single ACP monomer (Figure 3; also detected by size-exclusion chromotography). The ~2:1 (SKM:ACP) crosslinking ratio persists despite individually lengthening the incubation time, increasing the concentration of S^0KM and ACP, or changing the temperature, buffer, or the concentrations of the coupling enzymes CoaA, CoaD, CoaE,

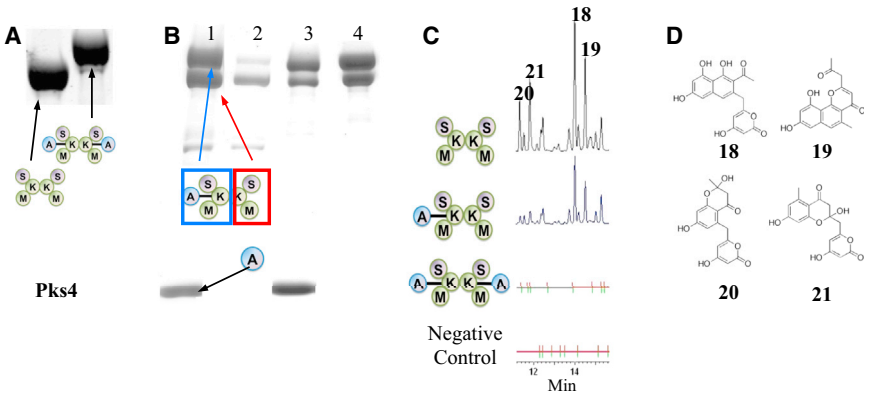

Figure 4. Composite Gels

(A) In comparison with Figure 3 (1 hr incubation), overnight incubation with doubling concentration of crosslinker and ATP, and triple concentration of ACP resulted in 100% crosslinking.

(B) Purification of Strep-tagged Pks4 ACP crosslinked to His-tagged Pks4 S^0KM. Lane 1: crosslinking reaction before purification steps. Lane 2: StrepTrap flowthrough indicates that excess S^0KM purified away from the crosslinked S^0KM = ACP. Lane 3: StrepTrap elution shows the resulting crosslinked S^0KM = ACP and its copurifying uncrosslinked S^0KM, plus contaminating Strep-tagged ACP. Lane 4: gel filtration-purified Pks4 S^0KM crosslinked to ACP.

(C) Pks4 in vitro reconstitution. The major products are PK8 (**18**), naphthopyrone (**19**), Sek4 (**20**), and Sek4b (**21**). All reactions are incubated with ACP and malonyl-CoA. In addition, reaction 1 contains pure SKM, reaction 2 contains pure, partially crosslinked SKM to ACP, reaction 3 contains fully crosslinked SKM to ACP, and reaction 4 has no protein present. Our hypothesis that crosslinking abolishes enzyme activity is supported by the result.

(D) Chemical structures of **18**–**21**.

and Sfp. In contrast, the S^0KM dimer is crosslinked to two monomers of ACP when the crosslinker and ATP concentrations are doubled, ACP concentration is tripled, 10% DMSO is added, and incubation time is extended to overnight (Figure 4A). The addition of DMSO improves overall protein solubility, while increasing ATP concentration may help increase the crosslinking efficiency, thus increasing the population of the doubly crosslinked species.

To ensure that the observed ~2:1 (SKM:ACP) ratio is not a result of the second KS being blocked by excess unloaded crosslinker or the coupling enzymes, we separated the crosslinker-loaded ACP (referred to as crypto-ACP) by fast protein liquid chromatography (FPLC; data not shown). Addition of purified crypto-ACP to S^0KM yielded a similar crosslinking result to the in situ reaction: the S^0KM:ACP ratio remains ~2:1, with similar overall efficiency. This control experiment confirms that the ~2:1 ratio is not a result of chemical interference but rather an inherent property of the ACP•KS complex.

To evaluate the enzymatic activity of the crosslinked S^0KM = ACP species ("=" denotes chemical crosslinking throughout the text), we conducted in vitro reconstitution assays using Pks4. S^0KM = ACP was generated and isolated by an orthogonal purification scheme (Figure 4B) (Haushalter et al., 2008). We crosslinked His-tagged Pks4 S^0KM to strep-tagged ACP. The reaction mixture was then passed through a StrepTrap FPLC column so that S^0KM = ACP and ACP were purified from the excess S^0KM and coupling enzymes CoaA, CoaD, CoaE, and Sfp (Figure 4B, lanes 2 and 3). The S^0KM = ACP and ACP mixture was then passed through a Superdex 200 size-exclusion column to separate ACP (MW = 16 kDa) from crosslinked S^0KM = ACP (MW = 298 kDa as the 2:1 complex). As expected, the purified S^0KM = ACP ran as a single band by native-PAGE, and analysis under denaturing conditions by SDS-PAGE showed that 50% of the S^0KM was the uncrosslinked species, which formed a dimer with crosslinked S^0KM and were carried through the purification process (Figure 4B, lane 4). The above result confirms the 2:1 S^0KM:ACP stoichiometry. We then conducted in vitro reconstitution assays to compare the product output of the 100% (2:2 S^0KM:ACP) and 50% (2:1 S^0KM:ACP) crosslinked S^0KM = ACP to an uncrosslinked S^0KM + ACP reaction (Figures 4C and 4D). The ACP concentration was standardized for each reaction. Because the SAT domain is mutated, starter units were provided by self-acylation of the KS domain under the high substrate conditions (Vagstad et al., 2012). We found that relative to the uncrosslinked reaction, only approximately 20% production (measured by high-performance liquid chromatography [HPLC] peak area) was detected for the 50% crosslinked S^0KM = ACP, supporting the view that (1) only one monomer of the S^0KM dimer is crosslinked to one ACP, and (2) the free S^0KM monomer is still capable of interacting with additional ACP in the solution. In comparison, the 100% crosslinked S^0KM = ACP completely lost its activity, supporting both S^0KM monomers as being blocked by the crosslinked ACPs.

Why can we only crosslink one ACP to one monomer of the S^0KM dimer unless the reaction conditions are pushed? Previously, crystal structures of porcine FAS and yeast FAS showed that although megasynthases, such as PKSs or FASs, exist as dimers in solution (Figure 2A), the two reaction chambers are in fact asymmetric (Maier et al., 2008; Rangan et al., 2001). Namely, as suggested by Rangan et al. (2001), the conformation of one subunit may trigger a corresponding change in its dimeric partner. Therefore, it is possible in NR-PKSs, that crosslinking of one monomeric ACP to one KS within the S^0KM dimer triggers a conformational change in the second S^0KM, resulting in a slower rate of complex formation with the second ACP. The free S^0KM only forms a stable complex with a second ACP after overnight incubation with a high concentration of crosslinker, ATP and ACP. This is also supported by the result in which 50% crosslinked S^0KM produces just 20% of product output compared to noncrosslinked S^0KM during in vitro reconstitution, rather than an expected 50% if no differences in the reactivity of the second monomer exist.

KS Mutations Identify Surface Residues Important for Protein·Protein Affinity

In order to visualize potential protein•protein interactions mediated by surface residues of KS and ACP, we generated homology models of Pks4 and PksA KS domains with Modeler (Fiser

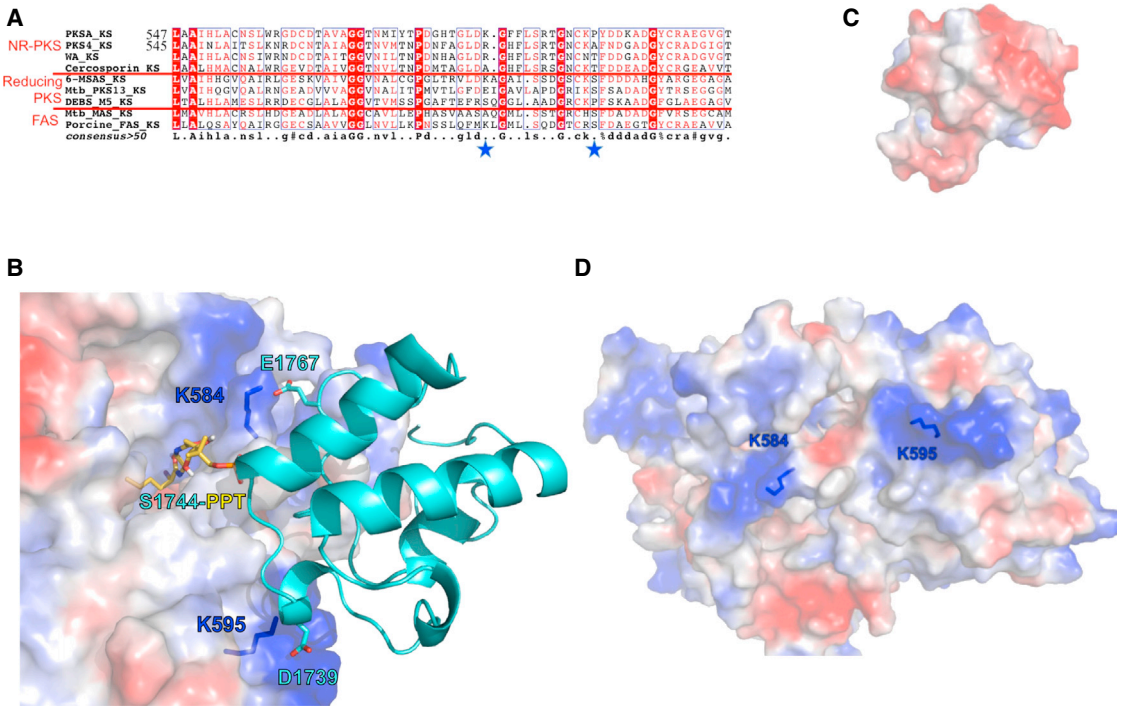

Figure 5. Probing Surface Residues Important for KS-ACP Interactions

(A) Sequence alignment identified two relatively conserved, positively charged residues (star). The boxed residues are conserved ones.

(B) Homology modeling and docking simulation of KS domains of PksA with PksA ACP suggests that K584 and K595 of PksA are located at the protein surface, where positively charged lysines are docked with acid residues of ACP, whereas active-site Ser tethered 2-bromohexyl pantetheine docks into the active site. D1739 and E1767 of PksA ACP were identified based on protein-protein docking simulation (Figure S7B).

(C) The negatively charged ACP surface that is docked to KS.

(D) The positively charged KS surface that is docked to ACP.

See also Figure S7.

and Šali, 2003), using DEBS KS5 as a template (Tang et al., 2006). The sequence identity between the KS domains of Pks4 and PksA is 57%, and the sequence identities between Pks4 KS and PksA A and DEBS KS5 are 31% and 34%, respectively. A >30% sequence identity is typically required for reliable homology modeling by Modeler (Fiser and Šali, 2003). We additionally conducted docking simulations of the 4'-phosphopantetheine analogs **15** and **16** to the KS active-site models, using the program GOLD (Verdonk et al., 2003). We found that the putative PPT binding pockets of the Pks4 and PksA KSs are highly conserved. Furthermore, when we compared the KS homology models, docking simulations, and sequence alignments (Figure 5A), we found that the 4'-phosphate of **15** and **16** consistently docked near residue K584 of PksA (corresponding to R582 of Pks4). Docking simulations between the PksA KS model and the PksA ACP structure (Wattana-amorn et al., 2010) further support that the positively charged surface created by K584 and K595 may be docked with the negatively charged surface of ACP (Figures 5B–5D). The PksA ACP residues D1739 and E1767 are each situated in close proximity to the KS residues, K595 and K584, respectively, and they may be involved in hydrogen bonding that contributes to ACP•KS interactions. Sequence alignment of NR-PKS ACP's indicates that D1739 is highly conserved among NR-PKS and the negative charge at residue 1767 is conserved in most NR-PKSs (Figure S7A). We hypothesize that the specificity between KS and ACP may require both electrostatic interactions between specific residues and overall protein conformation. Both lysines are located at the proposed substrate pocket entrance of KS (Figure 5D) and residues with positive polarity are relatively conserved across KS domains of different NR-PKSs at these positions (Figure 5A). The fact that the lysines are conserved among the KSs of NR-PKSs, but not other types of FASs and PKSs, supports the hypothesis that different types of megasynthases may have different residues that interact with their cognate ACPs. The above analysis leads to the hypothesis that K584 and K595 of PksA (R582 and K593 of Pks4, respectively) are important for protein•protein association between ACP and KS in NR-PKS.

To evaluate the importance of these surface lysines and arginine on ACP•KS interactions, we generated Ala, Glu, and Gln mutations for residues K584 and K595 of the PksA S^0KM and residues R582 and K593 of the Pks4 S^0KM. Circular dichroism experiments that compare the mutants to wild-type of both PKSA and PKS4 S^0KM indicate that the mutations do not significantly change the overall protein fold (Figures S5 and S6). The extent of crosslinking between these mutant S^0KMs and ACP was evaluated (Figure 3). We found that the charge reversing Glu mutations abolished crosslinking. In comparison, the neutral Ala mutants showed significantly diminished crosslinking, whereas the Gln mutants that preserve polarity maintained

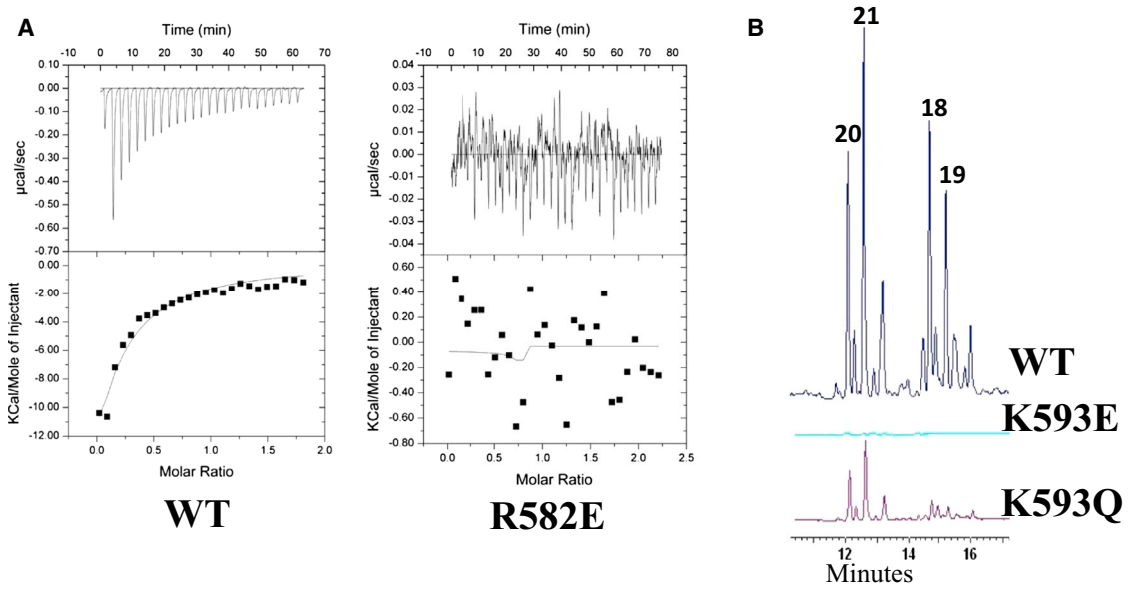

Figure 6. ITC and In Vitro Reconstitution Results that Compare Pks4 S^0KM with KS Surface Mutants

(A) ITC results show that interactions between Pks4 S^0KM wild-type and ACP are disrupted with the KS surface mutant R582E.

(B) Similarly, in vitro reconstitution shows that the surface mutant K593E disrupts interactions with ACP, whose in vitro activity is rescued by the K593Q mutant.

crosslinking. According to our model, polar residues at these positions appear to be important, such that a reversal of charge (the Lys or Arg to Glu mutants) abolished the interaction between the negatively charged ACP and the 4'-phosphate of pantetheine with the positively charged KS surface. However, if we maintain the polar character of the KS surface, in the case of the Lys or Arg to Gln mutation, a high degree of protein•protein affinity is maintained, resulting in high crosslinking efficiency. In support of the importance of polar (positively charged or noncharged) residues at these positions, eliminating the charge (the Lys to Ala mutants) does not eliminate crosslinking, but it severely decreases the crosslinking efficiency for PksA.

To validate that the observed crosslinking efficiency is, indeed, correlated with domain•domain association between ACP•KS and the PKS activity, we conducted isothermal titration calorimetry (ITC) and product analyses of in vitro reconstitution reactions from wild-type and mutant S^0KMs (Figure 6). By varying the concentration of S^0KM and ACP, we found that wild-type Pks4 S^0KM has an estimated K_D of 15 μM for Pks4 apo-ACP and 30 μM for PksA apo-ACP. In comparison, the Pks4 R582E mutant completely lost protein•protein interactions, and we could not measure its K_D (the dissociation constant between Pks4 ACP and S^0KM) by ITC (Figure 6A). Furthermore, the in vitro reconstitution assays with wild-type Pks4 S^0KM and Pks4 ACP resulted in the normal shunt products, **18**, **19**, **20**, and **21** (Figure 6B) (Ma et al., 2007), indicating that chain elongation is functional. In comparison, Pks4 K593E completely lost the ability to produce **18**–**21** (Figure 6B). This absence of polyketide extension and the loss of affinity by ITC for a single KS point mutant allow us to deduce that the ACP domain does not measurably bind either the SAT or MAT domains, and the NR-PKS resting state may be with the ACP docked to KS. Such an observation was made in the crystal structure of fungal FAS, where the holo-ACP and PPT were found to be "stalled" in the KS domain (Leibundgut et al., 2007). Alternatively, ACP may interact with SAT and MAT if it were in either the holo or acylated state. A third possibility is that certain conformational changes may need to occur via the holo or acylated form of ACP so that SAT or MAT may be allowed to interact with ACP. The above results offer strong support to correlate the observed difference in crosslinking efficiency between wild-type and mutant S^0KM with the strength of protein•protein interactions, which in turn is crucial for the biosynthesis of full-length polyketides. In addition, these results further reinforce the utility of crosslinking probes to provide a rapid readout for detecting docking interactions.

As further control experiments, in addition to the above mutants, we also generated Pks4 R546A, R546E, and R546Q, because R546 is also near the surface of the Pks4 KS active-site pocket. We found that these mutants do not change the crosslinking efficiency to the same degree as the other two mutants in Pks4 S^0KM (Figure S1). In summary, the above results confirm the importance of K584 and K595 of PksA (R582 and K593 of Pks4, respectively) to protein•protein interactions between KS and ACP domains, as well as correlate the ACP•KS interactions with polyketide biosynthetic activity.

Implications for Directing Biosynthesis: The ACP Specificity of NR-PKSs

A major goal of contemporary PKS research is to enable combinatorial biosynthesis, the process of mixing different enzyme domains to synthesize new products. To do so, maintenance of protein•protein interactions between ACP and other catalytic domains is essential (Mercer and Burkart, 2007). Although we showed that ACPs can be mixed with SKMs from different NR-PKSs, evaluating if such ACP promiscuity also extends to different types of PKSs and FASs is of significant interest. To

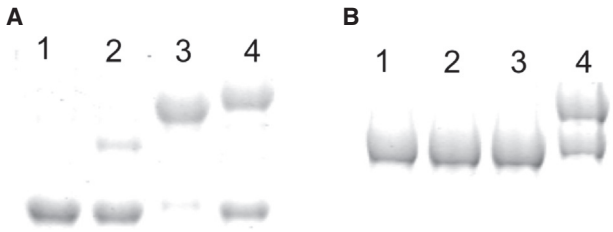

Figure 7. Crosslinking Gel with Type II ACP, Using Pantetheine Analog 15

(A) FabF crosslinked to the following ACPs: lane 1, negative control; lane 2, Act ACP; lane 3, AcpP; and lane 4, Pks4 ACP.

(B) Pks4 S^0KM that is crosslinked to the following ACPs: lane 1, negative control; lane 2, Act ACP; lane 3, AcpP; and lane 4, Pks4 ACP. The result showed that the KS-ACP pair is specific within the similar type of FAS or PKS.

more comprehensively evaluate ACP·KS interactions, we incubated ACP domains from a type II PKS (Act ACP) and a FAS (type II *E.coli* AcpP) with the S^0KM of either Pks4 or PksA and a crosslinker, either **15** for Pks4 or in the case of PksA S^0KM, **16** (Figure 7). As a positive control, we also included the matched pair, the *E. coli* type II ACP (AcpP) and KS (FabF). As expected, both type II ACPs, including the AcpP positive control, crosslink to FabF (Figure 7A); however, neither Act ACP nor AcpP crosslinks to the S^0KM of Pks4 or PksA (Figure 7B). Sequence alignment of ACP also shows that D1739 is conserved in both type I and II PKS ACPs, whereas E1767 is only conserved for NR-PKS ACPs. D1739 is located in the loop between helices I and II of ACP, whereas E1767 is located in helix III, a key region for ACP structural integrity and specificity with its partner proteins (Crosby and Crump, 2012). In the nuclear magnetic resonance structure by Wattana-amorn et al. (2010), helix III of an NR-PKS ACP is significantly different in orientation relative to ACPs of type II FASs and PKSs. In type II PKS and FAS ACPs, the residue aligned to PksA E1767 is uncharged (Figure S7A); therefore, both the specific charge-charge interactions and overall shape at the ACP-partner interface may be different between type I and type II ACPs. As Wattana-amorn et al. (2010) pointed out, the helix III region of NR-PKS is unusually hydrophobic when compared to ACPs from type II PKSs. Our docking simulation also supports the idea that hydrophobic residues of helix III from PksA ACP (such as F1771 and I1772) may form a hydrophobic interface with F586, F587 and L588 of the KS domain (Figure S7B). These hydrophobic residues are not conserved in type II PKSs (Figure S7A). A recent critical review by Crosby and Crump (2012) compared ACPs from type I and II FASs and PKSs in detail. The differences of charged residues and overall shape between the ACPs of NR-PKS and type II PKS may help explain how the NR-PKS KS·ACP partners are exchangeable among NR-PKSs, but not with type II PKSs (Figure 7). The above observation is also consistent with the report by Ma et al. (2006), who found that substituting the NR-PKS ACP into type II PKS results in significantly reduced PKS activity.

The above result has implications for downstream bioengineering efforts, in that NR-PKS ACPs can be mixed-and-matched with enzymes from other NR-PKSs, but not efficiently with type II FAS and PKS components. Previously, the fungal Pks1 and WA ACPs have also been reported to be interchangeable (Watanabe and Ebizuka, 2004). Similarly, Zhu et al. (2007) have reported successful swapping of fungal KS domains for the reducing fungal PKSs. These observations are in contrast to the previous report by Ma et al. (2006), who find that PksA ACP can be mixed with the type II actinorhodin ketosynthase/chain length factor to produce the type II shunt products, albeit with much reduced PKS activity. One likely explanation for such a difference is the nature of the architectures of type I and type II PKSs; whereas an NR-PKS needs to maintain a comparatively fixed architecture (Figure 2B) similar to the mammalian FAS (Figure 2A), a type II PKS consists of 5–10 stand-alone enzymes and does not have a stable organization. Consequently, the loosely associated type II PKS elongation machinery can accept a fungal ACP, but the organized NR-PKS machinery cannot accept the type II ACP, which presumably does not have a matching protein interface present in PksA and Pks4 ACPs. We conclude that for a successful project of combinatorial biosynthesis, the selection of a competent ACP is key to the maintenance of protein·protein interactions and intermediate transit between ACP and other enzyme domains.

SIGNIFICANCE

It is well recognized that protein·protein interactions must be important in transporting the starter unit, stabilizing, and sequestering the poly-β-keto intermediate and releasing the final cyclization product (Crawford and Townsend, 2010). However, only until our recent structural work on the NR-PKS PT (Crawford et al., 2009) and TE (Korman et al., 2010) and other's work on the ACP (Wattana-amorn et al., 2010) was it possible to appreciate the molecular interactions that result in orderly polyketide biosynthesis. Further, although there are more than 150 NR-PKS-containing gene clusters annotated (Li et al., 2010) and extensive phylogenetic analyses of the NR-PKSs (Kroken et al., 2003), these correlations do not identify residues important for protein·protein interactions essential for orchestrated domain function. Recognizing the need to probe for such interactions in the polyketide megasynthases, we used a simple and quick methodology by applying mechanism-based crosslinkers to probe the ACP·KS interactions in NR-PKSs. We found that ACPs from fungal NR-PKSs can be interchanged but that their KS domains do not accept ACPs from other types of PKSs or FASs, indicating the need of NR-PKSs to maintain their architecture (Figure 2B). We further found that the crosslinking efficiency is highly dependent on the chain length of the probe, reflecting the starter unit selectivity of the corresponding NR-PKSs (Figures 3A and 3B). Surface mutagenesis, in combination with crosslinking, ITC, and in vitro reconstitution experiments, further identified some residues important for ACP·KS interactions and established a strong correlation between domain docking and PKS activity. These results confirm the importance of protein·protein interaction in the NR-PKS complex. In the long run, knowledge about interdomain interactions in NR-PKSs can be applied to guide future biosynthetic efforts in the development of new "nonnative natural products" that can be screened for new biomedical activities.

EXPERIMENTAL PROCEDURES

Cloning and Mutagenesis

Plasmid pENKA-C117A that contained the *PksA* SAT-KS-MAT (S^0KM) C117A gene was cloned into pET28a(+), and pEPKS4-NKA-C117A that contained the *Pks4* S^0KM C117A gene was cloned into pET24a(+) (Vagstad et al., 2012). Finnzymes Phasing High-Fidelity DNA Polymerase was used in PCR to generate K582A, K582E, K582Q, K593A, K593E, and K593Q for pEPKS4-NKA-C117A, and R584A, R584E, R584Q, K595A, K595E, and K595Q for pENKA-C117A. *E. coli* strain NovaBlue (Novae) was used for plasmid amplification. All mutations were confirmed by sequencing. Primers were obtained from Integrated DNA Technologies. Specific primer sequences used included the following.

PKS4 SKM K582A Forward: 5′- GCCTCGATGCGGGGCATTTCCTTTCC CGTAC
PKS4 SKM K582A Reverse: 5′- ATGCCCCGCATCGAGGCCTGCAAAG TTGTCC
PKS4 SKM K582E Forward: 5′- GCCTCGATGAAGGGCATTTCCTT TCCCGTAC
PKS4 SKM K582E Reverse: 5′- ATGCCCTTCATCGAGGCCTGCAAAGT TGTCC
PKS4 SKM K582Q Forward: 5′- CCTCGATCAGGGGCATTTCCTT TCCCG
PKS4 SKM K582Q Reverse: 5′- GAAATGCCCCTGATCGAGGCCTG CAAAG
PKS4 SKM K593A Forward: 5′- GAAACTGCGCGGCTTTTAACGAC GGTGCGG
PKS4 SKM K593A Reverse: 5′- CGTTAAAAGCCGCGCAGTTTCCCGT ACGGG
PKS4 SKM K593E Forward: 5′- GGGAAACTGCGAAGCTTTTAACGA CGGTGCGG
PKS4 SKM K593E Reverse: 5′- CGTTAAAAGCTTCGCAGTTTCCCGT ACGGGAAAGG
PKS4 SKM K593Q Forward: 5′- GAAACTGCCAGGCTTTTAACGACG GTGCG
PKS4 SKM K593Q Reverse: 5′- CGTTAAAAGCCTGGCAGTTTCCCG TACGG
PKSA SKM K584A Forward: 5′- GATTGGACGCGGGGTTCTTTC TTTCCCGGAC
PKSA SKM K584A Reverse: 5′- GAACCCCGCGTCCAATCCTGTGTGA CCATC
PKSA SKM K584E Forward: 5′- GATTGGACGAAGGGTTCTTTCT TTCCCGG
PKSA SKM K584E Reverse: 5′- GAACCCTTCGTCCAATCCTGTG TGACC
PKSA SKM K584Q Forward: 5′- GATTGGACCAGGGGTTCTTTCTT TCCCGGAC
PKSA SKM K584Q Reverse: 5′- GAACCCCTGGTCCAATCCTGTGTGA CCATC
PKSA SKM K595A Forward: 5′- CAACTGCGCGCCCTACGACGACA AGGCCG
PKSA SKM K595A Reverse: 5′- GTAGGGCGCGCAGTTGCCAGTCCGGG AAAG
PKSA SKM K595E Forward: 5′- GCAACTGCGAACCCTACGACGAC AAGGCC
PKSA SKM K595E Reverse: 5′- GTAGGGTTCGCAGTTGCCAGTCCGG GAAAG
PKSA SKM K595Q Forward: 5′- GCAACTGCCAGCCCTACGACGA CAAGGCCG
PKSA SKM K595Q Reverse: 5′- CGTCGTAGGGCTGGCAGTTGC CAGTCCGG
PKSA SKM R546A Forward: 5′- CACCGCGCCTCTCGCAGACGC CCAGG
PKSA SKM R546A Reverse: 5′- GCGAGAGGCGCGGTGATGGAGAC GGAC
PKSA SKM R546E Forward: 5′- CACCGAACCTCTCGCAGACGC CCAGG
PKSA SKM R546E Reverse: 5′- GCGAGAGGTTCGGTGATGGAGAC GGAC
PKSA SKM R546Q Forward: 5′- ACCCAGCCTCTCGCAGACGCCCAGG
PKSA SKM R546Q Reverse: 5′- GCGAGAGGCTGGGTGATGGAGAC GGAC

Expression and Purification of His-Tagged Sfp, FabF, *apo*- ACP, and S^0KM Mutants

Plasmids pEACP41 and pEPKS4-ACP that contain the *PKSA* ACP and *PKS4* ACP genes, respectively, were cloned into pET28a(+) (Crawford et al., 2006). All plasmids were transformed into BL21 (DE3) cells. Transformed cells were grown by being shaken at 37°C in two 1 l of Luria-Bertani medium supplemented with 50 μg/ml kanamycin (or 50 μg/ml carbenecillin for Sfp) to an OD_{600} of 0.4–0.6. Protein expression was induced by the addition of 0.5 mM IPTG at 18°C overnight. The cells were harvested by centrifugation (5,000 rpm for 10 min at 4°C) and resuspended in 25 mM Tris-HCl (pH 8.0) at 4°C. The cells were pelleted, flash frozen in liquid nitrogen, and stored at −80°C until purification. Frozen cell pellets were defrosted on ice, resuspended in 40 ml lysis buffer (50 mM Tris-HCl [pH 7.5] at room temperature, 300 mM NaCl, 10% glycerol, and 20 mM Imidazole), and lysed by sonication (5 × 30 s pulses). The cell debris was removed by centrifugation (14,000 rpm for 1 hr at 4°C). Protein was bound to Ni-IMAC resin (Bio-Rad) by batch binding at 4°C for 1 hr. The lysis slurry was loaded onto a gravity column, where the lysate was eluted followed by 2 × 25 ml washes with lysis buffer. Protein was eluted at 40, 100, 150, 250, and 450 mM imidazole in lysis buffer to at least 95% purity. One millimolar 1,4-dithiothreitol (DTT) was added as elutions were collected. The purified protein was buffer exchanged overnight in 3 l dialysis buffer at 4°C with a 3 kDa (ACP) or 10 kDa (S^0KM and Sfp) Thermo Scientific Snakeskin membrane into 50 mM Tris-HCl (pH 8.0) at 4°C, 50 mM NaCl, 10% glycerol, and 1 mM DTT. The protein samples were concentrated between 4 and 10 mg/ml as determined by Bradford assay (Bio-Rad), flash frozen in liquid nitrogen, and stored at −80°C.

Expression and Purification of MBP-Tagged *E. coli* CoA Enzymes

The plasmids that contain MBP-tagged *E. coli* constructs *CoaA* (PanK), *CoaD* (PPAT), and *CoaE* (DPCK) were transformed into BL21 (DE3) cells (Haushalter et al., 2008). Transformed cells were grown by being shaken at 37°C in two 1 l of Luria-Bertani medium supplemented with 50 μg/ml carbenicillin and 0.2% (w/v) glucose to an OD_{600} of 0.4–0.6. Protein expression was induced by the addition of 0.5 mM IPTG at 18°C overnight. The cells were harvested by centrifugation (5,000 rpm for 10 min at 4°C) and resuspended in 25 mM Tris-HCl (pH 8.0) at 4°C. The cells were pelleted, flash frozen in LiN_2, and stored at −80°C until purification. Frozen cell pellets were defrosted on ice and resuspended in 40 ml lysis buffer (50 mM Tris-HCl [pH 7.5] at room temperature, 300 mM NaCl, 10% glycerol, 1 mM EDTA, and 1 mM DTT) and lysed by sonication (5 × 30 s pulses). The cell debris was removed by centrifugation (14,000 rpm for 1 hr at 4°C). Protein was bound to the amylose resin (NEB) by batch binding at 4°C for 1 hr. The lysis slurry was loaded onto a gravity column, where the lysate was eluted followed by 2 × 25 ml washes with lysis buffer. The protein was eluted at 1, 10, and 100 mM maltose in lysis buffer to at least 95% purity. The purified protein was buffer exchanged overnight in 3 l dialysis buffer at 4°C with a 10 kDa Thermo Scientific Snakeskin membrane into 50 mM Tris-HCl (pH 8.0) at 4°C, 10% glycerol, and 1 mM DTT. Protein samples were concentrated to 3 mg/ml as determined by Bradford assay (Bio-Rad), flash frozen in liquid nitrogen, and stored at −80°C.

Expression and Purification of Strep(II)-Tagged ACP Proteins

Plasmids pEACP41-SB and pEPKS4-SB that contain the *PKSA* ACP and *PKS4* ACP genes, respectively, were cloned into a modified pET-28a construct in which the N-terminal 6x-His tag was replaced by an N-terminal Strep(II) tag. All plasmids were transformed into BL21 (DE3) cells. Transformed cells were grown by being shaken at 37°C in two 1 l of Luria-Bertani medium supplemented with 50 μg/ml kanamycin to an OD_{600} of 0.4–0.6. Protein expression was induced by the addition of 0.5 mM IPTG at 18°C overnight. The cells were harvested by centrifugation (5,000 rpm for 10 min at 4°C) and resuspended in 25 mM Tris-HCl (pH 8.0) at 4°C. The cells were pelleted, flash frozen in liquid nitrogen, and stored at −80°C until purification. Frozen cell

pellets were defrosted on ice, resuspended in 40 ml lysis buffer (100 mM Tris-HCl (pH 7.5) at room temperature [RT], 200 mM NaCl, 1 mM DTT, and 1 mM EDTA), and lysed by sonication (5 × 30 s pulses). The cell debris was removed by centrifugation (14,000 rpm for 1 hr at 4°C), and protein was bound to a 5 ml StrepTrap FF column (GE), washed with 30 to 40 ml lysis buffer, and eluted with 2.5 mM d-desthiobiotin (Sigma-Aldrich) in lysis buffer. Column flowthrough and wash were combined and loaded on the column again, washed, and eluted from the StrepTrap column repeatedly until no protein was eluted from the column. The purified protein was buffer exchanged overnight in 3 l dialysis at 4°C with a 3 kDa Thermo Scientific Snakeskin membrane into 50 mM Tris-HCl (pH 8.0) at 4°C, 50 mM NaCl, 10% glycerol, and 1 mM DTT. Protein samples were concentrated to between 3 and 5 mg/ml as determined by Bradford assay (Bio-Rad), flash frozen in liquid nitrogen, and stored at −80°C.

Crosslinking of ACP and S^0KM, Resulting in Partial Crosslinking

Crosslinking probes **15**–**17** were prepared as previously described (Worthington et al., 2006; Worthington et al., 2008; Blatti et al., 2012). The loading of pantetheine analogs **15**–**17** to ACP was accomplished by combining a one-pot chemoenzyme reaction containing 50 mM Na phosphate (pH 7.0), 12.5 mM $MgCl_2$, 2 mM ATP, 15 μg/ml each of CoaA (250 nM), CoaD (200 nM), CoaE (300 nM), and Sfp (500 nM), 0.8 μg/μL ACP (50 μM), and 200 μM pantetheine analog (Haushalter et al., 2008). This reaction was incubated at 37°C for 1 hr. Pantetheine loading results were determined by MALDI-TOF. One micrograms/microliters S^0KM (7 μM) was added to the one-pot reaction and incubated an additional 1 hr at 37°C. Calculations were made so that the final volume after S^0KM addition was 50 μL. Samples were run on SDS-PAGE, using 7.5% Mini-PROTEAN TGX gels (Bio-Rad), to determine the extent of crosslinking.

Purification of Crosslinked S^0KM-ACP

Pure strep-tagged ACP and His-tagged S^0KM from PksA or Pks4 were crosslinked and purified as follows. A scaled-up crosslinking reaction to purify crosslinked protein was accomplished by combining a one-pot chemoenzyme reaction with 100 mM Na phosphate (pH 7.0), 12.5 mM $MgCl_2$, 2 mM ATP, 15 μg/ml each of CoaA (250 μM), CoaD (200 μM), CoaE (300 μM), and Sfp (500 μM), 0.8 mg/ml ACP (50 μM), and 200 μM pantetheine analog (Haushalter et al., 2008). This reaction was incubated at 37°C for 1 hr. One milligram/milliliter S^0KM (7 μM) was added to the one-pot reaction and incubated an additional 1 hr at 37°C. Calculations were made so that the final volume after S^0KM was added was between 5 and 20 ml. Protein was bound to a 5 ml StrepTrap FF column (GE), washed with 30 to 40 ml lysis buffer, and eluted with 2.5 mM d-desthiobiotin (Sigma-Aldrich) in lysis buffer. The StrepTrap column separated crosslinked S^0KM = ACP and uncrosslinked ACP from uncrosslinked S^0KM and chemoenzymes. The fractions were combined and concentrated to 10 mg/ml as determined by Bradford assay. The crosslinked S^0KM = ACP was separated from uncrosslinked ACP by gel filtration (Superdex 200, GE) in 25 mM Tris-HCl (pH 8.0) at 4°C and 1 mM DTT and concentrated to 5 mg/ml, where it was flash frozen using liquid nitrogen and stored at −80°C.

Crosslinking of ACP and S^0KM, Resulting in Complete Crosslinking

Crosslinking that resulted in 100% crosslinking utilized the same conditions as partial crosslinking with the following exceptions: 4 mM ATP, 2.5 μg/μL ACP (150 μM), and 500 μM pantetheine analog were used instead of the concentrations listed above. In addition, a final concentration of 10% DMSO was present during the reaction, and the reaction was carried out overnight at 37°C once S^0KM was added to the solution.

In Vitro Reconstitution

The in vitro reconstitution assays were prepared with 100 mM Tris-HCl (pH 7.5) at room temperature, 20 mM ATP (Sigma-Aldrich), 5 mM $MgCl_2$, 20 μM MatB, 5 mM CoA (Sigma-Aldrich), 50 μM *holo* PKS4 ACP, 10 μM PKS4 S^0KM or crosslinked protein as determined by Bradford assay, and 100 mM Na Malonate (Fisher), with a total final volume of 250 μL. The reaction tubes were left overnight in the dark. The reactions had 300 μl extraction solution (94:5:1 ethyl acetate:methanol:acetic acid) added to them, and they were then vortexed and centrifuged for 3 min at 14,000 rpm. The extraction layer was transferred to a fresh tube, where it was speed-vacuumed until dry. Each tube had 100 μl DMSO added to them, and they were stored at −20°C until analysis. Product analysis was performed by reverse-phase HPLC on a C18 analytical column (Phenomenex, 4 μm, 150 × 4.6 mm); 20 μl of the sample was loaded and separated with a 5% to 95% acetonitrile/0.1% formic acid gradient over 20 min with absorbance monitored by a UV-vis diode array detector tuned to 280 nm.

Docking In Silico

PKS4 and PKSA KS homology models were generated using DEBS KS5 (Protein Data Bank ID code 2HG4) from amino acids P40 to D457 as a template with the program Modeler (Fiser and Šali, 2003). GOLD was used to dock compounds to KS homology models (Verdonk et al., 2003).

Isothermal Calorimetry

Pure apo ACP and S^0KM or the S^0KM KS surface mutant proteins were buffer exchanged into the ITC buffer 50 mM Tris-HCl, 10% glycerol, and 50 mM NaCl with a PD-10 buffer-exchange column (GE Healthcare). The ACP protein was diluted to 200 μM and S^0KM, or the S^0KM KS surface mutants were diluted to 20 μM in ITC buffer. The ITC sample chamber was loaded with S^0KM or the KS surface mutants, and the sample syringe was loaded with ACP. The ITC was run with 25–10 μl injections of ACP with 150 s between injections. The K_ds were calculated by VPViewer 2000 (Micro Cal).

Circular Dichroism

Samples for circular dichroism (CD) experiments were prepared by diluting protein to 0.05–0.1 mg/ml in 20 mM Tris-HCl (pH 7.5), and the CD data were collected using a Jasco J810 CD spectropolarimeter.

SUPPLEMENTAL INFORMATION

Supplemental Information includes seven figures and can be found with this article online at http://dx.doi.org/10.1016/j.chembiol.2013.07.012.

Received: February 3, 2013
Revised: June 28, 2013
Accepted: July 7, 2013
Published: August 29, 2013

REFERENCES

Blatti, J.L., Beld, J., Behnke, C.A., Mendez, M., Mayfield, S.P., and Burkart, M.D. (2012). Manipulating fatty acid biosynthesis in microalgae for biofuel through protein-protein interactions. PLoS ONE *7*, e42949.

Cox, R.J. (2007). Polyketides, proteins and genes in fungi: programmed nano-machines begin to reveal their secrets. Org. Biomol. Chem. *5*, 2010–2026.

Crawford, J.M., and Townsend, C.A. (2010). New insights into the formation of fungal aromatic polyketides. Nat. Rev. Microbiol. *8*, 879–889.

Crawford, J.M., Dancy, B.C.R., Hill, E.A., Udwary, D.W., and Townsend, C.A. (2006). Identification of a starter unit acyl-carrier protein transacylase domain in an iterative type I polyketide synthase. Proc. Natl. Acad. Sci. USA *103*, 16728–16733.

Crawford, J.M., Thomas, P.M., Scheerer, J.R., Vagstad, A.L., Kelleher, N.L., and Townsend, C.A. (2008). Deconstruction of iterative multidomain polyketide synthase function. Science *320*, 243–246.

Crawford, J.M., Korman, T.P., Labonte, J.W., Vagstad, A.L., Hill, E.A., Kamari-Bidkorpeh, O., Tsai, S.C., and Townsend, C.A. (2009). Structural basis for biosynthetic programming of fungal aromatic polyketide cyclization. Nature *461*, 1139–1143.

Crosby, J., and Crump, M.P. (2012). The structural role of the carrier protein—active controller or passive carrier. Nat. Prod. Rep. *29*, 1111–1137.

Fiser, A., and Šali, A. (2003). Modeller: generation and refinement of homology-based protein structure models. Methods Enzymol. *374*, 461–491.

Haushalter, R.W., Worthington, A.S., Hur, G.H., and Burkart, M.D. (2008). An orthogonal purification strategy for isolating crosslinked domains of modular synthases. Bioorg. Med. Chem. Lett. *18*, 3039–3042.

Hopwood, D.A. (1997). Genetic contributions to understanding polyketide synthases. Chem. Rev. *97*, 2465–2498.

Huffman, J., Gerber, R., and Du, L. (2010). Recent advancements in the biosynthetic mechanisms for polyketide-derived mycotoxins. Biopolymers *93*, 764–776.

Kapur, S., Worthington, A., Tang, Y., Cane, D.E., Burkart, M.D., and Khosla, C. (2008). Mechanism based protein crosslinking of domains from the 6-deoxyerythronolide B synthase. Bioorg. Med. Chem. Lett. *18*, 3034–3038.

Kim, Y.T., Lee, Y.R., Jin, J., Han, K.H., Kim, H., Kim, J.C., Lee, T., Yun, S.H., and Lee, Y.W. (2005). Two different polyketide synthase genes are required for synthesis of zearalenone in Gibberella zeae. Mol. Microbiol. *58*, 1102–1113.

Korman, T.P., Crawford, J.M., Labonte, J.W., Newman, A.G., Wong, J., Townsend, C.A., and Tsai, S.C. (2010). Structure and function of an iterative polyketide synthase thioesterase domain catalyzing Claisen cyclization in aflatoxin biosynthesis. Proc. Natl. Acad. Sci. USA *107*, 6246–6251.

Kroken, S., Glass, N.L., Taylor, J.W., Yoder, O.C., and Turgeon, B.G. (2003). Phylogenomic analysis of type I polyketide synthase genes in pathogenic and saprobic ascomycetes. Proc. Natl. Acad. Sci. USA *100*, 15670–15675.

Leibundgut, M., Jenni, S., Frick, C., and Ban, N. (2007). Structural basis for substrate delivery by acyl carrier protein in the yeast fatty acid synthase. Science *316*, 288–290.

Li, Y., Image, I.I., Xu, W., Image, I., Tang, Y., and Image, I. (2010). Classification, prediction, and verification of the regioselectivity of fungal polyketide synthase product template domains. J. Biol. Chem. *285*, 22764–22773.

Linnemannstöns, P., Schulte, J., del Mar Prado, M., Proctor, R.H., Avalos, J., and Tudzynski, B. (2002). The polyketide synthase gene pks4 from Gibberella fujikuroi encodes a key enzyme in the biosynthesis of the red pigment bikaverin. Fungal Genet. Biol. *37*, 134–148.

Ma, Y., Smith, L.H., Cox, R.J., Beltran-Alvarez, P., Arthur, C.J., and Simpson F R S, T.J. (2006). Catalytic relationships between type I and type II iterative polyketide synthases: the Aspergillus parasiticus norsolorinic acid synthase. ChemBioChem *7*, 1951–1958.

Ma, S.M., Zhan, J., Watanabe, K., Xie, X., Zhang, W., Wang, C.C., and Tang, Y. (2007). Enzymatic synthesis of aromatic polyketides using PKS4 from Gibberella fujikuroi. J. Am. Chem. Soc. *129*, 10642–10643.

Maier, T., Leibundgut, M., and Ban, N. (2008). The crystal structure of a mammalian fatty acid synthase. Science *321*, 1315–1322.

Meier, J.L., Mercer, A.C., Rivera, H., and Burkart, M.D. (2006). Synthesis and evaluation of bioorthogonal pantetheine analogues for in vivo protein modification. J. Am. Chem. Soc. *128*, 12174–12184.

Meier, J.L., Haushalter, R.W., and Burkart, M.D. (2010). A mechanism based protein crosslinker for acyl carrier protein dehydratases. Bioorg. Med. Chem. Lett. *20*, 4936–4939.

Mercer, A.C., and Burkart, M.D. (2007). The ubiquitous carrier protein—a window to metabolite biosynthesis. Nat. Prod. Rep. *24*, 750–773.

Otten, S.L., Stutzman-Engwall, K.J., and Hutchinson, C.R. (1990). Cloning and expression of daunorubicin biosynthesis genes from Streptomyces peucetius and S. peucetius subsp. caesius. J. Bacteriol. *172*, 3427–3434.

Perlman, D., Heuser, L.J., Dutcher, J.D., Barrett, J.M., and Boska, J.A. (1960). Biosynthesis of tetracycline by 5-hydroxy-tetracycline-producing cultures of Streptomyces rimosus. J. Bacteriol. *80*, 419–420.

Petkovic, H., Hunter, I.S., and Raspor, P. (2002). Engineering of polyketide synthases: how close are we to the reality? Acta Microbiol. Immunol. Hung. *49*, 493–500.

Pickens, L.B., and Tang, Y. (2009). Decoding and engineering tetracycline biosynthesis. Metab. Eng. *11*, 69–75.

Rangan, V.S., Joshi, A.K., and Smith, S. (2001). Mapping the functional topology of the animal fatty acid synthase by mutant complementation in vitro. Biochemistry *40*, 10792–10799.

Rhodes, A., Boothroyd, B., McGONAGLE, P., and Somerfield, G.A. (1961). Biosynthesis of griseofulvin: the methylated benzophenone intermediates. Biochem. J. *81*, 28–37.

Shen, B. (2003). Polyketide biosynthesis beyond the type I, II and III polyketide synthase paradigms. Curr. Opin. Chem. Biol. *7*, 285–295.

Smith, S., Stern, A., Randhawa, Z.I., and Knudsen, J. (1985). Mammalian fatty acid synthetase is a structurally and functionally symmetrical dimer. Eur. J. Biochem. *152*, 547–555.

Tang, Y., Kim, C.Y., Mathews, I.I., Cane, D.E., and Khosla, C. (2006). The 2.7-Angstrom crystal structure of a 194-kDa homodimeric fragment of the 6-deoxyerythronolide B synthase. Proc. Natl. Acad. Sci. USA *103*, 11124–11129.

Vagstad, A.L., Bumpus, S.B., Belecki, K., Kelleher, N.L., and Townsend, C.A. (2012). Interrogation of global active site occupancy of a fungal iterative polyketide synthase reveals strategies for maintaining biosynthetic fidelity. J. Am. Chem. Soc. *134*, 6865–6877.

Verdonk, M.L., Cole, J.C., Hartshorn, M.J., Murray, C.W., and Taylor, R.D. (2003). Improved protein-ligand docking using GOLD. Proteins *52*, 609–623.

Watanabe, A., and Ebizuka, Y. (2004). Unprecedented mechanism of chain length determination in fungal aromatic polyketide synthases. Chem. Biol. *11*, 1101–1106.

Watanabe, C.M., Wilson, D., Linz, J.E., and Townsend, C.A. (1996). Demonstration of the catalytic roles and evidence for the physical association of type I fatty acid synthases and a polyketide synthase in the biosynthesis of aflatoxin B1. Chem. Biol. *3*, 463–469.

Wattana-amorn, P., Williams, C., Płoskoń, E., Cox, R.J., Simpson, T.J., Crosby, J., and Crump, M.P. (2010). Solution structure of an acyl carrier protein domain from a fungal type I polyketide synthase. Biochemistry *49*, 2186–2193.

Witkowski, A., Joshi, A.K., and Smith, S. (2004). Characterization of the beta-carbon processing reactions of the mammalian cytosolic fatty acid synthase: role of the central core. Biochemistry *43*, 10458–10466.

Worthington, A.S., and Burkart, M.D. (2006). One-pot chemo-enzymatic synthesis of reporter-modified proteins. Org. Biomol. Chem. *4*, 44–46.

Worthington, A.S., Rivera, H., Torpey, J.W., Alexander, M.D., and Burkart, M.D. (2006). Mechanism-based protein cross-linking probes to investigate carrier protein-mediated biosynthesis. ACS Chem. Biol. *1*, 687–691.

Worthington, A.S., Hur, G.H., Meier, J.L., Cheng, Q., Moore, B.S., and Burkart, M.D. (2008). Probing the compatibility of type II ketosynthase-carrier protein partners. ChemBioChem *9*, 2096–2103.

Worthington, A.S., Porter, D.F., and Burkart, M.D. (2010). Mechanism-based crosslinking as a gauge for functional interaction of modular synthases. Org. Biomol. Chem. *8*, 1769–1772.

Zhou, H., Li, Y., and Tang, Y. (2010). Cyclization of aromatic polyketides from bacteria and fungi. Nat. Prod. Rep. *27*, 839–868.

Zhu, X., Yu, F., Li, X.C., and Du, L. (2007). Production of dihydroisocoumarins in Fusarium verticillioides by swapping ketosynthase domain of the fungal iterative polyketide synthase Fum1p with that of lovastatin diketide synthase. J. Am. Chem. Soc. *129*, 36–37.

